European Journal of Mechanics / B Fluids 91 (2022) 1–8

Contents lists available at ScienceDirect

European Journal of Mechanics / B Fluids

journal homepage: www.elsevier.com/locate/ejmflu

Velocity–vorticity correlations and the four-layer regime in turbulent channel flow of generalized Newtonian fluids

Arturo A. Arosemena, Jannike Solsvik *

Department of Chemical Engineering, Norwegian University of Science and Technology (NTNU), NO 7491, Trondheim, Norway

ARTICLE INFO

Article history:
Received 9 February 2021
Received in revised form 2 August 2021
Accepted 28 August 2021
Available online 20 September 2021

Keywords:
Turbulence
Wall-bounded flow
Generalized Newtonian fluids
Low Reynolds number
Velocity–vorticity correlations
Four-layer dynamical regime

ABSTRACT

The data of Arosemena et al. (2021), consisting of turbulent channel flow simulations of generalized Newtonian (GN) fluids, are considered to study the effects of shear-dependent rheology on the nonzero velocity–vorticity correlations and the mean dynamics. In the near-wall region and compared to Newtonian channel flow, the velocity–vorticity products contributing to the turbulent inertia term decrease/increase with shear-thinning/thickening fluid behaviour suggesting that with e.g. shear-thinning rheology, the sublayer streaks are more stable, the near-wall vortical motions are dampened and there is a narrower range of turbulent length scales. The mean momentum balance analysis, on the other hand, revealed that the four-layer structure first recognized by Wei et al. (2005a) remains for all GN fluids and that the shear-dependent rheology only seems to influence the location of the layers. For instance, with shear-thinning behaviour, layers II and III are thicker and there is an increase in the importance of the viscous forces in these intermediate layers. The influence of shear-thinning/thickening fluid behaviour on the extent of the layers II and III is found remarkably similar to an increase/decrease of the Reynolds number for Newtonian channel flow. These findings suggest that the shear-dependent rheology should also be taken into account for proper scaling of the intermediate layers. A potential length scale factor is proposed and its suitability is tested.

1. Introduction

Turbulence is ubiquitous in nature and many man-made processes. Wall-bounded shear flows, such as boundary layers and pressure-driven pipes and channels, despite their simplicity in terms of geometrical configuration, are important reference flows for several technological applications. Consider, for instance, drag-related studies for novel designs of vehicles propelled in air and water, or the energy-budget analyses for a new generation of pipelines in the transport of gas and fuel within the petroleum industry.

Control of turbulence in wall-bounded flows for drag reduction, entrainment of particles or mixing purposes has concerned engineers and applied physicists for decades. The time-averaged form of the momentum equation differs from its instantaneous form since it involves a turbulence interaction term consisting of gradients of the net momentum flux $\rho u_i'$ by the macroscopic velocity fluctuations u_j'; here ρ is the density of the fluid. In an incompressible turbulent flow, the gradient of the turbulent or Reynolds stresses, $\partial\left(\overline{u_i'u_j'}\right)/\partial x_j$, can be rewritten as (see e.g. Hinze [1], Tardu [2])

$$\frac{\partial}{\partial x_j}\left(\overline{u_i'u_j'}\right) = \overline{u_j'\frac{\partial u_i'}{\partial x_j}} - \overline{u_j'\frac{\partial u_j'}{\partial x_i}} + \overline{u_j'\frac{\partial u_j'}{\partial x_i}} = -\overline{u_j'\omega_k'}\varepsilon_{ijk} + \frac{\partial}{\partial x_i}\left(\frac{\overline{u_j'u_j'}}{2}\right). \tag{1}$$

In the previous equation, mean and fluctuating variables are identified by $\overline{(\,)}$ and $(\,)'$, respectively, x_i and ω_i denote the spatial-Cartesian coordinates and the vorticity field, respectively, and ε_{ijk} is the alternation or Levi-Civita tensor. Note that, in Eq. (1), $\omega_k' = -\varepsilon_{ijk}\partial u_i'/\partial x_j$. Here, when index notation is used, suffix i (or any other suffix) takes the value 1,2 or 3 to represent the x, y or z component, respectively; i.e. $(x_1, x_2, x_3) = (x, y, z)$, $(u_1, u_2, u_3) = (u_x, u_y, u_z)$ and $(\omega_1, \omega_2, \omega_3) = (\omega_x, \omega_y, \omega_z)$, and a repeated index implies summation from x to z. Also, note that, we have adopted the common approach to denote the velocity correlation $\overline{u_i'u_j'}$ as the Reynolds stress tensor, which is not strictly correct.

For canonical channel flow, the $i = 1$–3 components of Eq. (1) read

$$-\frac{\partial}{\partial y}\left(\overline{u_x'u_y'}\right) = \overline{u_y'\omega_z'} - \overline{u_z'\omega_y'}, \tag{2}$$

* Corresponding author.
E-mail addresses: arturo.arosemena@ntnu.no (A.A. Arosemena), jannike.solsvik@ntnu.no (J. Solsvik).

https://doi.org/10.1016/j.euromechflu.2021.08.006

$$\frac{\partial k}{\partial y} = \overline{u_z'\omega_x'} - \overline{u_x'\omega_z'} + \frac{\partial}{\partial y}\left(\overline{u_y'u_y'}\right), \tag{3}$$

and

$$0 = \overline{u_y'\omega_x'} - \overline{u_x'\omega_y'}, \tag{4}$$

respectively. Here $k = \overline{u_i'u_i'}/2$ is the turbulent kinetic energy. For boundary layer, Eqs. (2)–(4) are approximately valid since the gradients $\partial\overline{(\,)}/\partial x$ are small but nonzero and become smaller relative to the other terms with increasing Reynolds number (Klewicki [3]). Thus, insight into how the stress gradients are generated can also be gained through the velocity–vorticity correlation terms, i.e., $\overline{u_j'\omega_k'}$.

Experimental and numerical investigations related to the velocity–vorticity products, and to turbulent–vorticity transport in general, are quite scarce (Eyink [4]). The studies by Klewicki and co-workers [3,5–8] are notable exceptions. Klewicki [3] used Eq. (1) and the approximate formulas of Phillips [9] to deduce some unmeasured (at that point) velocity–vorticity correlation profiles from available experimental data. The same study (Klewicki [3]) also showed that contributions to the gradients of the diagonal Reynolds stresses are dominated by the correlations involving the z-vorticity component whilst the contributions to the gradient of the off-diagonal stresses are shared between the correlations involving the z- and y-vorticity components. Klewicki et al. [5] considered zero-pressure-gradient boundary layer measurements to obtain the velocity–vorticity correlations and to investigate the ω_z' motion contributions to the gradients of the turbulent stresses and its possible relation to sweep and ejection events (Willmarth and Lu [10]; Wallace et al. [11]) in connection with important contributions to the turbulent diffusion term in the budget for $\overline{u_x'u_x'}$. Priyadarshana et al. [6] reported a number of statistics, based on laboratory data, related to the velocity–vorticity products including premultiplied cospectra and correlation coefficients and observed their sensitivity to Reynolds number as well to wall roughness. Klewicki et al. [7] pondered Eq. (2) in the context of the mean momentum balance-based layer structure for boundary layer, pipe and channel flows and their scaling behaviour (see Fife et al. [12,13]; Wei et al. [14,15]; Klewicki et al. [16,17]; Chin et al. [18]; White et al. [19], among others).

Afterwards, Morrill-Winter and Klewicki [8] focused on the $\overline{u_y'\omega_z'}$ correlation and its scale separation also in boundary layers, occurring as a function of both the y-coordinate and the Reynolds number, finding that the scaling of motions affiliated with the turbulent inertia term, i.e. $\partial\left(\overline{u_x'u_y'}\right)/\partial y$, is greater than $\mathcal{O}(\mu/(\rho u_\tau))$ in the region $y^+ = yu_\tau/(\mu/\rho) \leq 40$; where μ is the fluid's dynamic viscosity and $u_\tau = \sqrt{\overline{\tau}_w/\rho}$ is the frictional velocity defined in terms of the mean shear stress at the wall, $\overline{\tau}_w$. Aside from Klewicki and co-workers, it is worth mentioning the letter of Yoon et al. [20] who analysed the contributions of the velocity–vorticity correlations to the frictional drag in wall-bounded flows and found them dominant over the other contributions due to viscous and inhomogeneous effects in the x-direction (for boundary layer).

The aforementioned studies, concerning the velocity–vorticity products, are mostly about canonical wall-bounded flows of Newtonian fluids despite that for many industrial applications, the working fluid is non-Newtonian. The purpose of this paper is to explore the effects of shear-dependent rheology on the velocity–vorticity correlations in a turbulent channel flow and the underlying physical implications. As mentioned before, there are but a few studies regarding the velocity–vorticity interaction terms and to the authors' knowledge, none where the effect of having non-constant, nonelastic viscosity is considered. Moreover, our interest not only lays in the changes of the correlations but also in how such changes affect the net mean effect of turbulent inertia and the resulting mean momentum balance in the wall-bounded flow. The study of the redistribution of mean momentum clarifies the influence of shear-dependent rheology over the mean dynamics and potentially leads to a proper scaling of this type of non-Newtonian channel flow.

2. The numerical experiments

Velocity–vorticity correlations and other statistics are computed using data from turbulent channel flow simulations of GN fluids at a frictional Reynolds number, $Re_\tau = \rho u_\tau h/\mu_w = 180$; h being the channel half-width and μ_w the nominal wall viscosity based on $\overline{\tau}_w$ and the considered rheology model (see Draad et al. [21]; Ptasinski et al. [22]). GN fluids are purely viscous, time independent fluids which stress tensor due to viscous effects, $\tau_{ij_{\text{vis}}}$, is given by

$$\tau_{ij_{\text{vis}}} = 2\mu S_{ij}, \tag{5}$$

where $\mu = \mu(\dot{\gamma})$ is the apparent dynamic viscosity solely depending on the strain rate $\dot{\gamma} = \left(2S_{ij}S_{ji}\right)^{1/2}$ and $S_{ij} = \left(\partial u_i/\partial x_j + \partial u_j/\partial x_i\right)/2$ is the strain rate tensor. The rheology of a GN fluid may be reproduced through different models such as the power-law (PL), Spriggs or Carreau fluid models (see e.g. Irgens [23]) which relate the apparent viscosity to the strain rate through a constitutive equation. The choice of a particular model has little effect on the turbulent flow predictions if high strain rate rheology (typical in turbulent regime near walls) is used in the rheology characterization (Singh et al. [24]).

The direct numerical simulations (DNS) are performed using a FORTRAN 77 code called CALC-LES (Davidson and Peng [25]; Davidson [26]) which solves the incompressible form of the momentum and continuity equations through a finite volume method on a collocated grid, using central differencing approximations in space and the Crank–Nicolson scheme in time. The numerical procedure consists of an implicit, two-time stepping technique where the Poisson's equation for the pressure is solved with an efficient multigrid method (Emvin [27]). Regarding boundary conditions, in the wall-normal direction (y-coordinate) physical (no-slip, impermeable) top and bottom walls are imposed and periodicity is set in the streamwise/longitudinal (x-coordinate) and spanwise/lateral (z-coordinate) directions of the computational box.

In the DNS, to avoid unphysical results at large and low strain rate values which may arise with the simpler PL fluid model, the rheology is incorporated through the Carreau model, i.e.,

$$\mu = \mu_\infty + (\mu_0 - \mu_\infty)\left[1 + (\Lambda\dot{\gamma})^2\right]^{(\alpha-1)/2}, \tag{6}$$

where μ_∞ and μ_0 are the 'infinite' and 'zero' shear rate viscosities, respectively, Λ is a time constant and α is the flow index which for shear-thinning/thickening is to be less/more than unity. Here, the different parameters are adjusted to attain the target Re_τ according to the set nominal wall viscosity. Fig. 1 shows the mean (averaged in time and in the spatially homogeneous directions) viscosity for the considered shear-thinning/pseudoplastic (P180), Newtonian (N180) and shear-thickening/dilatant (D180) fluids cases. As evidenced by Eq. (6), shear-thinning/thickening refers to a fluid exhibiting a decrease/increase in its apparent fluid viscosity with increasing strain rate. It is remarked that at the given flow conditions and within the region where viscous effects are likely dominant, the increase/decrease of local viscosity with shear-thinning/thickening behaviour is (on average) less than 50% of the approximate value at the wall. Such increase/decrease is comparable to what has been reported in previous studies

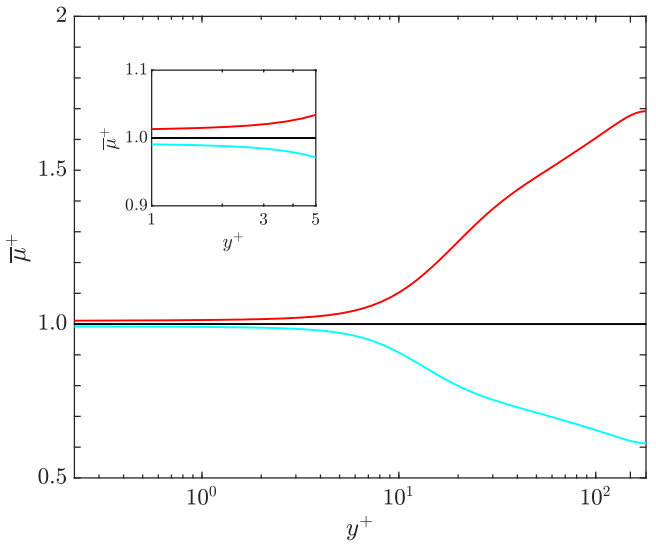

Fig. 1. Mean viscosity profile, $\overline{\mu}^+ = \mu/\mu_w$, vs. y^+. Here, $\mu_\infty/\mu_0 = 1 \times 10^{-3}$, $\mu_0^+ \approx 1.782/0.561$ for fluid case P180/D180, $\Lambda^+ = 0.1$ and α is set to 0.8, 1.0 and 1.2 for fluid cases P180, N180 and D180, respectively. Profiles corresponding to P180, N180 and D180 are identified by red, black and cyan colours, respectively. (For interpretation of the references to colour in this figure legend, the reader is referred to the web version of this article.)

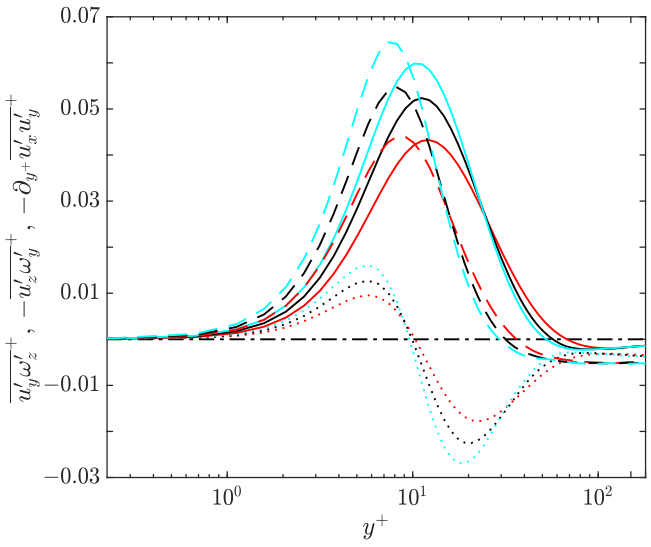

Fig. 2. Contributions to the wall-normal gradient of the Reynolds stress, $-\partial\left(\overline{u'_x u'_y}^+\right)/\partial y^+$, and wall-normal gradient of the Reynolds stress vs. y^+. Line styles "–" and "· · ·" are used to identify contributions from the correlations $-\overline{u'_z\omega'_y}^+$ and $\overline{u'_y\omega'_z}^+$, respectively, whereas line style "- - -" is used for the gradient $-\partial_{y^+}\overline{u'_x u'_y}^+ = -\partial\left(\overline{u'_x u'_y}^+\right)/\partial y^+$ and line style "- · -" for the zero-crossing line. Profiles corresponding to fluid cases P180, N180 and D180 are identified by red, black and cyan colours, respectively. (For interpretation of the references to colour in this figure legend, the reader is referred to the web version of this article.)

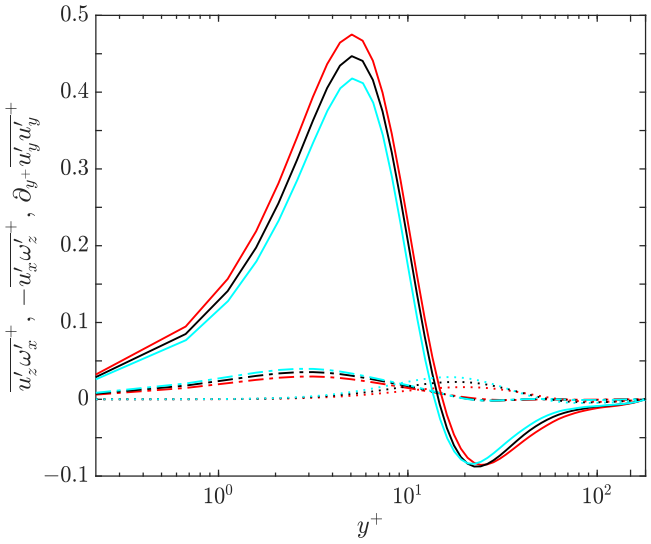

Fig. 3. Contributions to the wall-normal gradient of the turbulent kinetic energy, $\partial k^+/\partial y^+$, vs. y^+. Line styles "–", "- · -" and "· · ·" are used to identify contributions from the correlations $-\overline{u'_x\omega'_z}^+$, $\overline{u'_z\omega'_x}^+$ and the gradient $\partial_{y^+}\overline{u'_y u'_y}^+ = \partial\left(\overline{u'_y u'_y}^+\right)/\partial y^+$, respectively. Profiles corresponding to fluid cases P180, N180 and D180 are identified by red, black and cyan colours, respectively. (For interpretation of the references to colour in this figure legend, the reader is referred to the web version of this article.)

(see viscosity rheograms in e.g. Rudman et al. [28]; Gavrilov and Rudyak [29]; Singh et al. [30]). Note as well that, the channel flow is pressure-driven and that all turbulent scales have been properly resolved for the simulations of the three considered GN fluid cases. For further details regarding the computational set-up and the used database, we refer to Arosemena et al. [31].

In the following sections, most statistics are given in 'wall' units, $(\,)^+$, using $\mu_w, u_\tau, (\mu_w/\rho)/u_\tau, (\mu_w/\rho)/u_\tau^2$ and ρu_τ^2 as characteristic viscosity, velocity, length, time and stress, respectively.

3. Velocity–vorticity correlations

Figs. 2 and 3 show the contributions to the wall-normal gradient of the nonzero Reynolds stresses, i.e., terms on the right-hand side of Eqs. (2) and (3), respectively. As it can be seen from Fig. 2, for the considered GN fluid cases, contributions to the gradient of the off-diagonal component, $\partial\left(\overline{u'_x u'_y}^+\right)/\partial y^+$, are shared by correlations involving both ω'_z and ω'_y; the interaction term $-\overline{u'_z\omega'_y}$, in particular, appears to dominate the most within the region $y^+ \lesssim 30$. The relative contributions of these correlations to the turbulent inertia term are clarified by taking their ratio; see Fig. 4. The figure also displays the wall-normal position, y_m^+, at which a maximum is attained for the Reynolds shear stress, i.e., the zero-crossing point of its wall-normal gradient. As seen from Fig. 4, at y_m^+ the ratio $\overline{u'_y\omega'_z}/\overline{u'_z\omega'_y} \approx 1$ whereas prior/beyond y_m^+, the correlation $\overline{u'_y\omega'_z}$ becomes smaller/larger than the $-\overline{u'_z\omega'_y}$ term. On the other hand, Fig. 3 reveals that, for all considered GN fluid cases, contributions to the gradient of the diagonal stresses are dominated by the correlation involving ω'_z. The interaction terms appearing in Eq. (4), found to be several orders of magnitude less than $\overline{u'_z\omega'_x}$ which is the smallest velocity–vorticity product studied so far (see Fig. 3), are considered approximately zero. Thus, for all cases, the wall-normal and streamwise velocity components appear to be uncorrelated to the longitudinal and wall-normal vorticity components, respectively.

The velocity–vorticity correlations presented in Fig. 2 are particularly important since their difference not only expresses the mean effect of turbulent inertia in the differential statement of mean dynamics (Morrill-Winter and Klewicki [8]) but also, their cross-stream gradients are the source or sink for the mean vorticity (Tennekes and Lumley [32]). The correlation $\overline{u'_y\omega'_z}$ is related to the advective transport, central to Taylor's mixing-length theory of vorticity transfer [33], and it has been shown to be particularly relevant for the development of the logarithmic

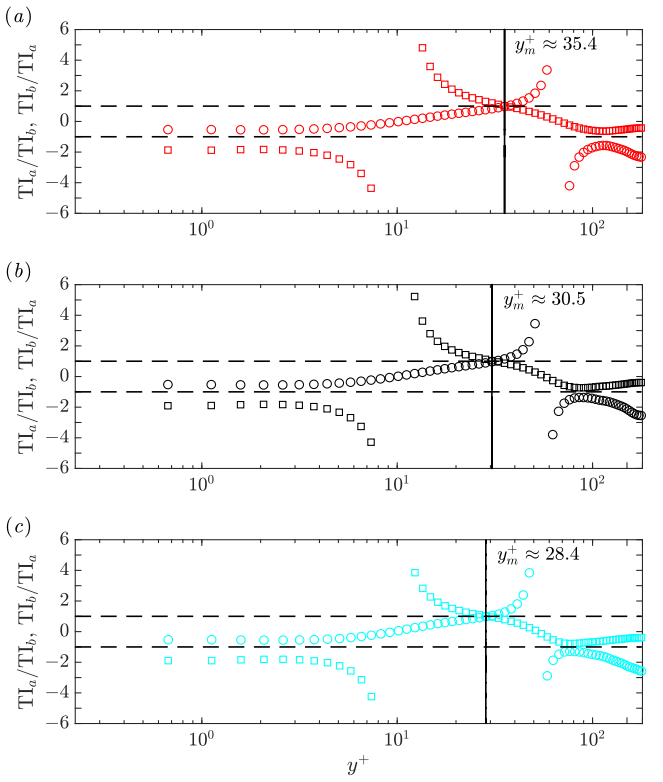

Fig. 4. Ratios of the velocity–vorticity correlations, $\mathrm{TI}_a/\mathrm{TI}_b$ and $\mathrm{TI}_b/\mathrm{TI}_a$, vs. y^+; here $\mathrm{TI}_a = \overline{u_y'\omega_z'}$ and $\mathrm{TI}_b = \overline{u_z'\omega_y'}$. In (*a*)-(*c*), profiles corresponding to fluid cases P180, N180 and D180 are identified by red, black and cyan coloured markers, respectively. The marker '∘' is used for the $\mathrm{TI}_a/\mathrm{TI}_b$ ratio whilst the marker '□' is used for the $\mathrm{TI}_b/\mathrm{TI}_a$ ratio. (For interpretation of the references to colour in this figure legend, the reader is referred to the web version of this article.)

mean velocity profile (Klewicki et al. [16]) once the leading order terms in the mean dynamics are purely inertial (Wei et al. [14]). On the other hand, the correlation $\overline{u_z'\omega_y'}$ is related to change-of-scale effects (Tennekes and Lumley [32]), constitute a gain (or loss) of mean vorticity in the channel flow—note that total production of $\overline{\omega}_z$ is given by $\overline{\omega_j'\partial u_z'/\partial x_j} = \partial\left(\overline{\omega_j' u_z'}\right)/\partial x_j$ since ω_j' is divergenceless— and when it is not negligible implies that the mixing-length theory is not an appropriate approximation. In Fig. 2, the peaks in the correlations occur near $y^+ \approx 5-10$ where the wall-normal gradients of $-\overline{u_x' u_y'}^+$ are the largest. Also, close to the peak values and with shear-thinning/thickening fluid rheology, the absolute value of the correlations decrease/increase which is consistent with the overall decrease/increase of turbulent shear stress and its wall-normal gradient with shear-thinning/thickening fluid behaviour (see the mean shear stress budget in e.g. Singh et al. [30]). Here, an interesting observation is that both velocity–vorticity products are affected by the shear-dependent rheology. This is in contrast with the observed changes due to Reynolds number for Newtonian wall-bounded flow where only the correlation $\overline{u_z'\omega_y'}$ appears to be Reynolds-number-dependent (Chin et al. [18]). Meanwhile, unsurprisingly and as shown in Fig. 3, the principal contribution to $\partial k^+/\partial y^+$ also attains its maximum close to the edge of the viscous sublayer, $y^+ \approx 5$, and increases/decreases with shear-thinning/thickening fluid behaviour. This interaction term involves u_x'—largest velocity fluctuation— and ω_z'—important source for the sustainment of turbulence—which intensities are known to increase/decrease with shear-thinning/thickening fluid rheology in the very near-wall region (see e.g. Arosemena et al. [31]).

At this point, we would like to highlight the (potential) physical implications of changes observed with shear-dependent rheology in the velocity–vorticity correlations contributing to the turbulent inertia term. The region of positive $\overline{u_y'\omega_z'}$, seen up to $y^+ \approx 10$ (compared to the Newtonian case, actual zero-crossing point slightly increases/decreases with shear-thinning/thickening behaviour as displayed in Fig. 2), is believed to be related to the outward motion of sublayer streaks (Klewicki et al. [5]) whereas the region of negative $\overline{u_y'\omega_z'}$, after $y^+ \approx 10$, is believed to be due to the vertical advection of detached hairpin-like vortex heads; likely important for the near-wall self-sustaining process of vortical motion (Falco et al. [34]; Klewicki et al. [5]). In consequence, compared to a Newtonian fluid and with e.g. shear-thinning fluid behaviour, the suppression of $\overline{u_y'\omega_z'}$ across the channel seems to imply that the sublayer streaks are more stable, i.e., less prone to be lifted-up, oscillate and eventually break-up during a 'bursting' process (Kim et al. [35]; Offen and Kline [36]) and that the strength of the near-wall vortical motions is reduced. See contours of instantaneous streamwise velocity fluctuations, u_x', in e.g. Singh et al. [37]; Arosemena et al. [31], where coarser structures with less 'streakiness', more streamwise coherence and larger spanwise separation are observed with shear-thinning rheology and Arosemena et al. [31], where the intensity of the streamwise vorticity component is reported to decrease—for the shear-thinning fluid— when compared to the Newtonian base case.

Related to one of the previous remarks, it is worth comparing the changes experienced by the near-wall streaks in Newtonian channel flow due to a decrease in Reynolds number with those attributed to shear-thinning rheology. In Newtonian fluids where the flow is wall-bounded, the streaks are known to keep a relatively constant spanwise spacing (see e.g. Klewicki et al. [38]; Cossu and Hwang [39]) but the bursting periods are longer (see e.g. Jímenez et al. [40]). The fact that, for a Newtonian fluid, the bursting period seems to increase with decreasing Re_τ does not imply an increase in stability in the same sense as for shear-thinning behaviour, i.e. structures less prone to be lifted-up, but that perhaps due to the lessened turbulence intensity (see e.g. Lee and Moser [41]), the streaks are likely to persist over longer periods of time. Furthermore, as aforementioned, the correlation associated with the outward motion of the streaks ($\overline{u_y'\omega_z'}$) appears nearly invariant to changes of Reynolds number. On the other hand, with respect to the term $-\overline{u_z'\omega_y'}$ associated with the modulation (change-of-scale effect) of near-wall motions, its overall attenuation—for the shear-thinning fluid case— is a clear indicative of a decrease in the range of length scales in the turbulent channel flow. See the previously mentioned contours of u_x' in Singh et al. [37]; Arosemena et al. [31], where a narrower range of turbulent eddy sizes is observed for the shear-thinning fluid compared to the Newtonian fluid and also, Section 4.1; about the hierarchy of length scales.

Finally, it would be wise to discuss the possible Reynolds number dependency of the velocity–vorticity correlations and related statistics. At least up to moderate frictional Reynolds numbers ($Re_\tau = 750$), contribution of viscosity fluctuations (in e.g. the mean shear budget or the turbulent kinetic energy budget) are known to remain relatively small and consistent trends in the different statistics (including the Reynolds shear stress which wall-normal gradient is directly related to the terms $\overline{u_y'\omega_z'}$ and $-\overline{u_z'\omega_y'}$) are seen when comparing Newtonian and shear-dependent fluid cases (Singh et al. [37]). In consequence, at least up to moderate Reynolds numbers, a similar Re_τ dependency (for the different statistics) is deem probable for all GN fluid cases. In other words, it is likely that for a particular GN fluid, an increase in Reynolds number would lead to an invariant $\overline{u_y'\omega_z'}$-profile whereas the correlation $-\overline{u_z'\omega_y'}$ is expected to display a

similar Reynolds number dependency to the turbulent inertia term as reported by Chin et al. [18] for Newtonian wall-bounded flow. It is emphasized that this last statement elucidates what the authors find probable and should be taken with caution. Definite evidence about the Reynolds number dependency of the velocity–vorticity products for GN fluids in wall-bounded turbulent flows requires actual computation of these profiles for a wide range of Reynolds numbers and it is proposed as further work.

4. Streamwise mean momentum balance and the four-layer structure

Based on the properties of the mean velocity profile and the mean shear stress field, turbulent boundary layer, channel and pipe flows are commonly scaled according to identified regions consisting of different layers (see e.g. Tennekes and Lumley [32]; Pope [42]): there is an inner layer region; comprised by a viscous sublayer $\left(y^+ \lesssim 5\right)$, a buffer layer region $\left(5 \lesssim y^+ \lesssim 30\right)$, a log-law region $\left(30 \lesssim y^+ \lesssim 0.15h^+\right)$, and a remaining outer region. There is some discrepancy in the location of the layers reported by different authors and in general, the logarithmic-law layer, overlapping the inner and outer regions, is more distinct as the Reynolds number increases (see e.g. Smits et al. [43]; Marusic et al. [44]). Wei et al. [14] remarked that it is the gradients of the stresses and not the stresses themselves that are the relevant dynamical quantities and proposed an alternative layer structure directly based on the mean dynamics described by the time-averaged momentum balance. As a framework, before discussing the mean dynamics for the shear-dependent cases, we briefly outline the mean momentum equation analysis for turbulent channel flow of GN fluids which (as presented) is indistinct to the one of Newtonian channel and pipe flows and fairly similar to the one of zero-pressure-gradient turbulent boundary layer; see for instance Fife et al. [12]; Wei et al. [14]; Klewicki et al. [17]; Chin et al. [18], among others.

For a statistically converged, pressure-driven, turbulent channel flow of a GN fluid, the streamwise mean momentum equation reads

$$\frac{\partial}{\partial y^+}\left(\overline{u_x' u_y'}\right)^+ = \frac{1}{Re_\tau} + \frac{\partial}{\partial y^+}\left(\overline{\tau}_{xy_{\text{vis}}}^+\right), \tag{7}$$

since the mean continuity equation and the y-component of the mean momentum equation lead to $-\partial\overline{p}^+/\partial x^+ = -\mathrm{d}\overline{p}_w^+/\mathrm{d}x^+ = \overline{\tau}_w^+/h^+$ which by definition is equivalent to $1/Re_\tau$. Here p denotes pressure and the subscript 'w' refers to values at the bottom wall of the channel. In general, for a GN fluid, the total mean viscous shear stress is given by $\overline{\tau}_{xy_{\text{vis}}}^+ = 2\left[\overline{\mu}^+\overline{\mathrm{S}}_{xy}^+ + \left(\overline{\mu' \mathrm{S}_{xy}'}\right)^+\right]$; i.e., $\overline{\tau}_{xy_{\text{vis}}}^+$ may also include a contribution arising due to viscosity fluctuations. In terms of simpler notation, Eq. (7) can be rewritten as

$$\mathrm{TI} = \mathrm{PG} + \mathrm{VF}. \tag{8}$$

Hence, for the channel flow, the mean statement of dynamics indicates that the net effect of turbulent inertia (TI) is balanced by the sum of the mean pressure gradient (PG) and net viscous force (VF). Based on Eq. (8), for $Re_\tau \geq 180$, Wei et al. [14] noted that indeed the three effects must all be in balance, or have at least two non-negligible terms in balance, and recognized that the mean dynamical balance can be described by a four-layer structure: layer I, $|\mathrm{PG}| \approx |\mathrm{VF}| \gg |\mathrm{TI}|$; layer II, $|\mathrm{VF}| \approx |\mathrm{TI}| \gg |\mathrm{PG}|$; layer III, $|\mathrm{PG}| \approx |\mathrm{VF}| \approx |\mathrm{TI}|$; layer IV, $|\mathrm{PG}| \approx |\mathrm{TI}| \gg |\mathrm{VF}|$.

Fig. 5, displaying the terms appearing in Eq. (8), reveals the mean dynamics for turbulent channel flow of the considered GN fluid cases. In the figure, the net mean viscous force is split into $\mathrm{VF}^{(\mathrm{N})} = 2\left(\overline{\mu}^+\overline{\mathrm{S}}_{xy}^+\right)$ and $\mathrm{VF}^{(\mathrm{NN})} = 2\left(\overline{\mu' \mathrm{S}_{xy}'}\right)^+$, being the last term non-zero only for the shear-dependent cases since it arises due to fluctuations in viscosity. As seen from Fig. 5, in the near-wall region and for all cases, the turbulent inertia term is balanced out by $\mathrm{VF}^{(\mathrm{N})}$ with an error $\mathrm{VF}^{(\mathrm{NN})} + \mathrm{PG}$. Furthermore, as mentioned while discussing Fig. 2, with shear-thinning/thickening fluid behaviour the peak value in $-\mathrm{TI}$ is suppressed/enhanced and moves slightly to the right/left in comparison with the Newtonian case. Also, as already seen from Fig. 4, the zero-crossing point of the turbulent inertia term (y_m^+) appears to be affected by the shear-dependent rheology; with shear-thinning/thickening, the wall-normal position at which $\mathrm{TI} = 0$ occurs further/nearer the wall in comparison with the Newtonian fluid case. On the other hand, the term arising due to fluctuation in viscosity $\left(\mathrm{VF}^{(\mathrm{NN})}\right)$ peaks in magnitude near the upper edge of the traditional viscous sublayer, i.e. $y^+ \approx 5$, and seems to be in favour/against $-\mathrm{TI}$ for shear-thinning/thickening fluid rheology. Nonetheless, $\mathrm{VF}^{(\mathrm{NN})}$ approaches zero as we move further away from the wall and, across the channel, its magnitude is always smaller than the magnitude of the normalized, constant, driving pressure gradient. In summary, the inherent character of the mean dynamics seems to remain the same for all GN fluids and the shear-dependent rheology appears to only influence the location of the regions depending on the leading-order balance between the terms in Eq. (8).

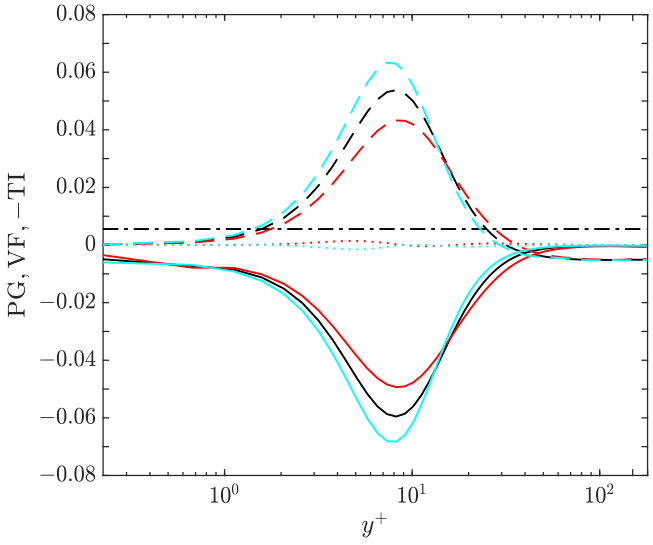

Fig. 5. Distribution of stress gradients in the Reynolds-averaged streamwise momentum equation vs. y^+. Line styles "- · -" , "—", "· · ·" and "- - -" are used to identify PG, $\mathrm{VF}^{(\mathrm{N})}$, $\mathrm{VF}^{(\mathrm{NN})}$ and −TI, respectively. Profiles corresponding to fluid cases P180, N180 and D180 are identified by red, black and cyan colours, respectively. (For interpretation of the references to colour in this figure legend, the reader is referred to the web version of this article.)

Following Wei et al. [14], the regions corresponding to the four-layer structure are revealed through the −VF/TI ratio shown in Fig. 6. The inner viscous/pressure-gradient balance layer (layer I), extending from the wall up to $y^+ \approx 3$, does not differ in a significant manner from the traditional viscous sublayer and appears to be unaffected by the shear-dependent rheology in terms of its physical extent but does display a larger |VF/TI| ratio with shear-thinning fluid behaviour. At the outer edge of layer I, the ratio −VF/TI approaches −1 and marks the beginning of the stress-gradient balance layer (layer II). Note that, at low Reynolds numbers for pressure-driven channel flow, the ratio of −1 is approached asymptotically, probably, due to a net diminishing effect of the associate surface flux of vorticity (Wei et al. [14]). Layer II extends up to a wall-normal position where the ratio −VF/TI is less than −2 (Wei et al. [14]) and marks the start of

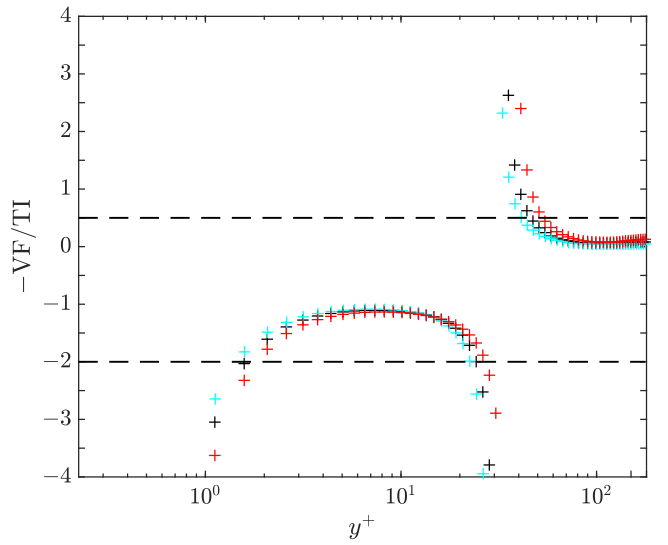

Fig. 6. Ratio of the mean viscous force to the mean effect of turbulent inertia, −VF/TI, vs. y^+. Profiles corresponding to fluid cases P180, N180 and D180 are identified by red, black and cyan coloured markers, respectively. (For interpretation of the references to colour in this figure legend, the reader is referred to the web version of this article.)

the viscous/pressure-gradient/inertial balance layer (layer III). In layer III, TI changes sign at y_m^+ and Eq. (8) undergoes a balance breaking and exchange of terms (Klewicki et al. [7]); i.e., in the mean force balance, the turbulent inertia starts to be of leading order instead of the mean viscous force (Morrill-Winter and Klewicki [8]). Finally, the inertial/pressure-gradient balance layer (layer IV) is attained when the ratio −VF/TI decreases to 0.5 (Wei et al. [14]) and marks the beginning of an inertial subrange where viscous forces can be neglected. As seen from Fig. 6, layers II and III appear to be thicker/thinner with shear-thinning/thickening fluid behaviour in comparison to the Newtonian case and thus, the influence of VF appears to increase/decrease up to wall-normal positions further away from/closer to the wall with shear-thinning/thickening rheology. Moreover, such behaviour is probably due to the local increase/decrease of viscosity as y^+ increases for the shear-thinning/thickening cases; see Fig. 1. This clearly contrasts with the results reported for viscoelastic channel flow (White et al. [19]); where, even for the low drag reduction regime (Warholic et al. [45]), the increase of importance in the viscous effects—compared to Newtonian channel flow and as we move further away from the wall— is attributed not to an increase in viscosity but to a diminishing importance of the inertial effects.

It is also worth remarking that the effect of shear-thinning/thickening rheology in the −VF/TI profile seems to be similar to an increase/decrease of the Reynolds number in the Newtonian case (see e.g. Klewicki et al. [17]) which suggests that proper scaling of the intermediate layers in turbulent channel flow of GN fluids should account for their shear-dependency. In Section 4.1, scaling concepts are applied to identify the (potential) appropriate length scales in the different regions and to gain further insight into the four-layer structure once the shear-dependent rheology is introduced. The analysis follows the conceptual framework used by Fife et al. [12,13] in which the stress gradient balance layers have a mathematical structure composed of a hierarchy of length scales and, where, the traditional inner and outer scales are simply the two extremes in a continuum of length scales.

4.1. The hierarchy of length scales

Consider Eq. (7) in the following convenient form

$$\frac{\mathrm{dV}}{\mathrm{d}y^+} + \frac{\mathrm{dT}}{\mathrm{d}y^+} + \epsilon^2 = 0, \tag{9}$$

where $\mathrm{V}\left(y^+\right) = \overline{\tau}_{xy_{\mathrm{vis}}}^+$, $\mathrm{T}\left(y^+\right) = -\overline{u_x' u_y'}$ and $\epsilon^2 = 1/Re_\tau$. Also, consider a mathematical construct, based on the Reynolds shear stress, defined as

$$\mathrm{T}^\beta\left(y^+\right) = \mathrm{T}\left(y^+\right) + \epsilon^2 y^+ - \beta y^+. \tag{10}$$

Here T^β is an adjusted Reynolds stress (in T^β, β is a superscript not an exponent) and β is a small positive number restricted to $\beta \leq \left[\max\left(\mathrm{dT}/\mathrm{d}y^+\right) + \epsilon^2\right]/C$; where the coefficient C is a number in the interval 5 to 20 (Fife et al. [12]). Note that, the function T^β satisfies

$$\frac{\mathrm{dT}^\beta}{\mathrm{d}y^+} = \frac{\mathrm{dT}}{\mathrm{d}y^+} + \epsilon^2 - \beta, \tag{11}$$

and thus, Eq. (9) can be rewritten as

$$\frac{\mathrm{dV}}{\mathrm{d}y^+} + \frac{\mathrm{dT}^\beta}{\mathrm{d}y^+} + \beta = 0. \tag{12}$$

As will be seen shortly, the introduction of T^β allow us to have an exact differential equation in rescaled variables with no explicit dependency on any parameter. Moreover, T^β has led to Eq. (12) expressing an approximate balance between its first two terms for an arbitrary (small) β-parameter. Such balance must be (eventually) broken, at a given y^+, and changes to another kind of balance where the three terms in Eq. (12) have the same order of magnitude (Fife et al. [12]; Fife [46]).

Proper scaling of Eq. (12)—in a given region—requires that the two derivatives are bounded and at least one of them cannot be too small. Through a transformation of differentials, such as

$$\mathrm{d}y^+ = \ell \mathrm{d}\hat{y}, \quad \mathrm{dV} = \phi \mathrm{d}\hat{\mathrm{V}}, \quad \mathrm{dT}^\beta = \delta \mathrm{d}\hat{\mathrm{T}}^{\hat{\beta}}, \tag{13}$$

it is possible to rescale the original variables into the new variables $\hat{y}$, $\hat{\mathrm{V}}$ and $\hat{\mathrm{T}}^{\hat{\beta}}$ which (potentially) represent most clearly and naturally the momentum balance within a certain subdomain of interest. The coefficients ℓ, ϕ and δ in the linear transformations are β-dependent. In consequence, with the use of the differential transformations (13), Eq. (12) is recast as

$$\left(\frac{\phi}{\ell}\right)\frac{\mathrm{d}\hat{\mathrm{V}}}{\mathrm{d}\hat{y}} + \left(\frac{\delta}{\ell}\right)\frac{\mathrm{d}\hat{\mathrm{T}}^{\hat{\beta}}}{\mathrm{d}\hat{y}} + \beta = 0. \tag{14}$$

A suitable scaling would render the previous differential equation (14) into a parameterless equation. This requires matching, in formal order of magnitude, between the two terms involving derivatives in Eq. (14) and the third term, β. Therefore, one can specify

$$\ell = \frac{\phi}{\beta}, \quad \delta = \phi. \tag{15}$$

As seen from Eq. (15), the criterion of equal order of magnitude, by itself, does not define uniquely the three scaling factors since, for a given β, one of them is still undetermined. A possible closure is found assuming that e.g. $\phi\,(\beta) = \beta^{-\sigma}$; where the parameter σ is an exponent (Fife [46]). Hence

$$\ell = \beta^{-(\sigma+1)}, \quad \delta = \phi = \beta^{-\sigma}. \tag{16}$$

If $\beta = \epsilon^2$, inner and outer length scaling are recovered for $\sigma = -1$ and $\sigma = 0$, respectively. The continuum of scales is between these two extreme cases, i.e., $\sigma \in [-1, 0]$ when $\beta = \epsilon^2$.

The intermediate or 'meso' layer III in Wei et al. [14] corresponds to $\sigma = -1/2$ and $\beta = \epsilon^2$. However, this mesolayer III is

Table 1
Scaling behaviour of the intermediate layer III for turbulent channel flow of GN fluids. Here, $\Delta y^+_{\mathrm{III}} = y^+_3 - y^+_2$; where y^+_2 and y^+_3 denote the beginning and end of mesolayer III.

Case	$\Delta y^+_{\mathrm{III}}$	$\mu^+\left(y^+_m\right)$	$\Delta y^+_{\mathrm{III}}/\sqrt{Re_\tau \mu^+\left(y^+_m\right)}$
D180	18.6	0.75	1.60
N180	22.1	1	1.65
P180	26.2	1.41	1.64

just one among many, in the sense that, different adjusted mesolayers can be constructed by replacing T by T^β and mesolayer III is just a particular case, where $\mathrm{T}^\beta = \mathrm{T}$, and which approximate centre is at the location $y^+ = y^+_m$ where the balance breaking and exchange of leading-order terms in the streamwise mean momentum equation occurs (Fife et al. [12]). Note as well that, when $\beta = \epsilon^4$, $\sigma = -1/2$ and $\mathrm{T}^\beta \neq \mathrm{T}$ also corresponds to the outer length scaling case.

At this point, it is worth mentioning that the previous observations are valid for all GN fluids however, the fact that local variations of viscosity take place for the shear-dependent cases, and in the light of results presented in Fig. 6– where the extension of the intermediate layers seems to be affected by the shear-dependent rheology–make us ponder if the choice $\sigma = -1/2$ and $\beta = \epsilon^2$ is the most suitable for layer III. Considering that the balance breaking in Eq. (8) happens at $y^+ = y^+_m$, where TI = 0 (see Fig. 4), another reasonable candidate for the parameter of interest, β, would be $\epsilon^2/\overline{\mu}^+\left(y^+_m\right)$; i.e., a rescaling factor which takes into account the increase/decrease of the mean viscosity (with respect to nominal μ_w) at $y^+ = y^+_m$ for the shear-thinning/thickening fluid case. For the Newtonian case, as remarked earlier, the intermediate layer is centred in the vicinity of y^+_m since $\mathrm{dT}/\mathrm{d}y^+ = \mathrm{dT}^\beta/\mathrm{d}y^+ = 0$. In contrast, for the shear-thinning and shear-thickening fluid cases is centred around $y^+ = y^+_\beta$ where $\mathrm{dT}^\beta/\mathrm{d}y^+ = 0$. This wall-normal position, for the considered cases, is nearby y^+_m. In comparison with y^+_m, y^+_β is slightly closer to/further away from the wall for the shear-thickening/thinning case since the location of the maximum for T^β decreases as β increases. In consequence, for the shear-dependent cases, $\overline{\mu}^+\left(y^+_\beta\right)$ is expected to be slightly larger than $\overline{\mu}^+\left(y^+_m\right)$ but not to significantly affect the proposed scaling, in particular, as $\epsilon^2 \to 0$, i.e., as the frictional Reynolds number increases.

The suitability of the choice $\beta = \epsilon^2/\overline{\mu}^+\left(y^+_m\right)$ for turbulent channel flow of GN fluids can be checked in a quantitative manner. Based on the transformations (13), we obtain $y^+_3 - y^+_2 = \beta^{-1/2}\left(\hat{y}_3 - \hat{y}_2\right)$; where y^+_2 and y^+_3 denote the beginning and end of mesolayer III, respectively, and $\hat{y}_2$ and $\hat{y}_3$ the same wall-normal positions but now in the rescaled variable. Here, $\Delta\hat{y} = \hat{y}_3 - \hat{y}_2 = \mathcal{O}(1)$ and thus, $\Delta y^+ = y^+_3 - y^+_2 = \mathcal{O}\left(\beta^{-1/2}\right)$. As seen from Table 1, the ratio $\Delta y^+/\sqrt{Re_\tau \mu^+\left(y^+_m\right)}$ appears to bounded for all GN fluid cases, and, it is expected that will tend to 1 as Re_τ increases, i.e., as $\epsilon^2 \to 0$. Note as well that this decrease/increase in the overall range of length scales with shear-thinning/thickening fluid behaviour is in line with the showed trends for $-\overline{u'_z\omega'_y}$ in Section 3.

5. Summary

Turbulent channel flow simulations of GN fluids, consisting of weakly shear-thinning, Newtonian, and weakly shear-thickening fluid cases, at $Re_\tau = 180$ (Arosemena et al. [31]) are considered to compute the nonzero velocity–vorticity correlations and some statistics related to the mean dynamics.

Regarding the velocity–vorticity products, for all considered GN fluid cases, contributions to the wall-normal gradient of $-\overline{u'_x u'_y}$ are shared between the vortex-stretching and advective transport terms, i.e., $-\overline{u'_z\omega'_y}$ and $\overline{u'_y\omega'_z}$, respectively. On the other hand, contributions to the wall-normal gradient of the turbulent kinetic energy are dominated by the correlation $-\overline{u'_x\omega'_z}$ which, in the near-wall region, seemingly increases/decreases in magnitude with shear-thinning/thickening fluid behaviour. The opposite trend is noted for the velocity–vorticity products related to the turbulent inertia term, suggesting that with e.g. shear-thinning rheology, the sublayer streaks are more stable, the near-wall vortical motions are dampened, and there is a narrower range of turbulent eddy sizes.

In the context of mean momentum balance analysis, for the shear-dependent cases, the contributions $\mathrm{VF}^{(\mathrm{NN})}$ (arising due to fluctuations in viscosity) are found to peak in the vicinity of the wall but, across the channel, are always smaller than PG and overall are deemed negligible. The study of the terms contributing to the mean momentum balance revealed that the four-layer structure, first recognized by (Wei et al. [14]), remains for all GN fluids and that the shear-dependent rheology appears to only influence the location of the layers. Compared to Newtonian channel flow, with shear-thinning/thickening fluid behaviour, the upper bound for layers II and III are located further away/closer to the wall and with e.g. shear-thinning rheology, the balance breaking and exchange of mean forces at y^+_m also moves further away from the channel wall. The results imply an increase/decrease in the importance of the viscous forces in the intermediate layers with shear-thinning/thickening behaviour.

We remark that the effect of shear-dependent rheology on the thickness of layer II and III is strikingly similar to a change of Reynolds number for Newtonian channel flow (see e.g. Klewicki et al. [17]; Chin et al. [18]) which strongly suggests that the shear-dependency should be taken into account for proper scaling of the intermediate layers in wall-bounded flows of GN fluids. The mean momentum balance-based layers have a mathematical structure composed of a hierarchy of length scales (Fife et al. [12]) and for the intermediate layer III, in case of shear-dependent rheology, it is proposed that a suitable length scale should account for the local variation in the mean viscosity (with respect to its nominal wall value) at y^+_m. Quantitative evidence (see Table 1) revealed that the width of the mesolayer III, $\Delta y^+_{\mathrm{III}}$, seems to scale with $\sqrt{Re_\tau \mu^+\left(y^+_m\right)}$ which is in line with the previous observation about the overall decrease/increase in the range of turbulent length scales with shear-thinning/thickening rheology in the channel flow.

Declaration of competing interests

The authors declare that they have no known competing financial interests or personal relationships that could have appeared to influence the work reported in this paper.

Acknowledgements

This work was supported by the Research Council of Norway (RCN, Grant No. 274398). The authors are grateful for computer resources provided by NTNU IDUN/EPIC computing cluster (Själander et al. [47]).

References

[1] J. Hinze, Turbulence, McGraw-Hill, 1975.
[2] S. Tardu, Statistical Approach to Wall Turbulence, Wiley-ISTE, 2011.
[3] J.C. Klewicki, Velocity–vorticity correlations related to the gradients of the Reynolds stress in parallel turbulent wall flows, Phys. Fluids A 1 (1989) 1285–1289, http://dx.doi.org/10.1063/1.857354.

[4] G.L. Eyink, Turbulent flow in pipes and channels as cross-stream "inverse cascades" of vorticity, Phys. Fluids 20 (2008) 125101, http://dx.doi.org/10.1063/1.3013635.
[5] J.C. Klewicki, J. Murray, R.E. Falco, Vortical motion contributions to stress transport in turbulent boundary layers, Phys. Fluids 6 (1994) 277–286, http://dx.doi.org/10.1063/1.868082.
[6] P.A. Priyadarshana, J.C. Klewicki, S. Treat, J.F. Foss, Statistical structure of turbulent-boundary layer velocity-vorticity products at high and low Reynolds numbers, J. Fluid Mech. 570 (2007) 307–346, http://dx.doi.org/10.1017/S0022112006002771.
[7] J. Klewicki, P. Fife, T. Wei, P. McMurty, A physical model of the turbulent boundary layer consonant with mean momentum balance structure, Phil. Trans. R. Soc. A 365 (2007) 823–839, http://dx.doi.org/10.1098/rsta.2006.1944.
[8] C. Morrill-Winter, J. Klewicki, Influences of boundary layer scale separation on the vorticity transport contribution to turbulent inertia, Phys. Fluids 25 (2013) 015108, http://dx.doi.org/10.1063/1.4775361.
[9] W.R.C. Phillips, The wall region of a turbulent boundary layer, Phys. Fluids 30 (1987) 2354–2361, http://dx.doi.org/10.1063/1.866125.
[10] W.W. Willmarth, S.S. Lu, Structure of the Reynolds stress near the wall, J. Fluid Mech. 55 (1972) 65–92, http://dx.doi.org/10.1017/S002211207200165X.
[11] J.M. Wallace, H. Eckelmann, R.S. Brodkey, The wall region in turbulent shear flow, J. Fluid Mech. 54 (1972) 39–48, http://dx.doi.org/10.1017/S0022112072000515.
[12] P. Fife, T.W.J. Klewicki, P. McMurty, Stress gradient balance layers and scale hierarchies in wall bounded turbulent flows, J. Fluid Mech. 532 (2005) 165–189, http://dx.doi.org/10.1017/S0022112005003988.
[13] P. Fife, J. Klewicki, P. McMurty, T. Wei, Multiscaling in the presence of indeterminacy: wall-induced turbulence, Multiscale Model. Simul. 4 (2005) 936–959, http://dx.doi.org/10.1137/040611173.
[14] T. Wei, P. Fife, J. Klewicki, P. McMurty, Properties of the mean momentum balance in turbulent boundary layer, pipe and channel flows, J. Fluid Mech. 522 (2005) 303–327, http://dx.doi.org/10.1017/S0022112004001958.
[15] T. Wei, P. McMurty, J. Klewicki, P. Fife, Meso scaling of the Reynolds shear stress in turbulent channel and pipe flows, AIAA J. 43 (2005) 2350–2353, http://dx.doi.org/10.2514/1.15617.
[16] J. Klewicki, P. Fife, T. Wei, On the logarithmic mean profile, J. Fluid Mech. 638 (2009) 73–93, http://dx.doi.org/10.1017/S002211200999084X.
[17] J. Klewicki, C. Chin, H.M. Blackburn, A. Ooi, I. Marusic, Emergence of the four layer dynamical regime in turbulent pipe flow, Phys. Fluids 24 (2012) 045107, http://dx.doi.org/10.1063/1.3702897.
[18] C. Chin, J. Philip, J. Klewicki, A. Ooi, I. Marusic, Reynolds-number-dependent turbulent inertia and onset of log region in pipe flows, J. Fluid Mech. 757 (2014) 747–769, http://dx.doi.org/10.1017/jfm.2014.486.
[19] C.M. White, Y. Dubief, J. Klewicki, Properties of the mean momentum balance in polymer drag-reduced channel flow, J. Fluid Mech. 834 (2018) 409–433, http://dx.doi.org/10.1017/jfm.2017.721.
[20] M. Yoon, J. Ahn, J. Hwang, H.J. Sung, Contribution of velocity–vorticity correlations to the frictional drag in wall-bounded turbulent flows, Phys. Fluids 28 (2016) 081702, http://dx.doi.org/10.1063/1.4961331.
[21] A.A. Draad, G.D.C. Kuiken, F.T.M. Nieuwstadt, Laminar-turbulent transition in pipe flow for Newtonian and non-Newtonian fluids, J. Fluid Mech. 377 (1998) 267–312, http://dx.doi.org/10.1017/S0022112098003139.
[22] P.K. Ptasinski, F.T.M. Nieuwstadt, B.H.A.A. Van Der Brule, M.A. Hulsen, Experiments in turbulent pipe flow with polymer additives at maximum drag reduction, Flow Turbul. Combust. 66 (2001) 159–182, http://dx.doi.org/10.1023/A:1017985826227.
[23] F. Irgens, Rheology and Non-Newtonian Fluids, Springer, 2014, http://dx.doi.org/10.1007/978-3-319-01053-3.
[24] J. Singh, M. Rudman, H.M. Blackburn, A. Chryss, L. Pullum, L.J.W. Graham, The importance of rheology characterization in predicting turbulent pipe flow of generalized Newtonian fluids, J. Non-Newton. Fluid Mech. 232 (2016) 11–21, http://dx.doi.org/10.1016/j.jnnfm.2016.03.013.
[25] L. Davidson, S.-H. Peng, Hybrid LES-RANS: A one-equation SGS model combined with a k-ω for predicting recirculating flows, Internat. J. Numer. Methods Fluids 43 (9) (2003) 1003–1018, http://dx.doi.org/10.1002/fld.512.
[26] L. Davidson, CALC-LES: A Fortran code for LES and hybrid LES-RANS, Technical Report, Chalmers University of Technology, 2020, URL http://www.tfd.chalmers.se/~lada/postscript_files/calc-les.pdf.
[27] P. Emvin, The Full Multigrid Method Applied to Turbulent Flow in Ventilated Enclosures Using Structured and Unstructured Grids (Ph.D. thesis), Chalmers University of Technology, Gothenburg, 1997.
[28] M. Rudman, H.M. Blackburn, L.J.W. Graham, L. Pullum, Turbulent pipe flow of shear-thinning fluids, J. Non-Newton. Fluid Mech. 118 (2004) 33–48, http://dx.doi.org/10.1016/j.jnnfm.2004.02.006.
[29] A.A. Gavrilov, V.Y. Rudyak, Direct numerical simulation of the turbulent flows of power-law fluids in a circular pipe, Thermophys. Aeromech. 23 (2016) 473–486, http://dx.doi.org/10.1134/S0869864316040016.
[30] J. Singh, M. Rudman, H.M. Blackburn, The influence of shear-dependent rheology on turbulent pipe flow, J. Fluid Mech. 822 (2017) 848–879, http://dx.doi.org/10.1017/jfm.2017.296.
[31] A.A. Arosemena, H.I. Andersson, J. Solsvik, Turbulent channel flow of generalized Newtonian fluids at a low Reynolds number, J. Fluid Mech. 908 (2021) A43, http://dx.doi.org/10.1017/jfm.2020.903.
[32] H. Tennekes, J.L. Lumley, A First Course in Turbulence, MIT Press, 1972.
[33] G.I. Taylor, The transport of vorticity and heat through fluids in turbulent motion, Proc. R. Soc. Lond. Ser. A Math. Phys. Eng. Sci. 135 (1932) 685–701, http://dx.doi.org/10.1098/rspa.1932.0061.
[34] R.E. Falco, J.C. Klewicki, K. Pan, Production of turbulence in boundary layers and potential for modification of the near-wall region, in: A. Gyr (Ed.), Structure of Turbulence and Drag Reduction, Springer-Verlag, Berlin Heidelberg, 1990, pp. 59–67, http://dx.doi.org/10.1007/978-3-642-50971-1_4.
[35] H.T. Kim, S.J. Kline, W.C. Reynolds, The production of turbulence near a smooth wall in a turbulent boundary layer, J. Fluid Mech. 50 (1971) 133–160, http://dx.doi.org/10.1017/S0022112071002490.
[36] G.R. Offen, S.J. Kline, A comparison and analysis of detection methods for the measurement of production in a boundary layer, in: Proc. 3rd Biennial Symposium of Turbulence in Liquids, University of Missouri-Rolla, 1973, pp. 289–320, URL http://scholarsmine.mst.edu/sotil/119.
[37] J. Singh, M. Rudman, H.M. Blackburn, Reynolds Number effects in pipe flow turbulence of generalized Newtonian fluids, Phys. Rev. Fluids 3 (2018) 094607, http://dx.doi.org/10.1103/PhysRevFluids.3.094607.
[38] J. Klewicki, M.M. Metzger, E. Kelner, E.M. Thurlow, Viscous sublayer flow visualizations at $R_\theta \approx 150\,000$, Phys. Fluids 7 (1995) 857–863, http://dx.doi.org/10.1063/1.868763.
[39] C. Cossu, Y. Hwang, Self-sustaining processes at all scales in wall-bounded turbulent shear flows, Phil. Trans. R. Soc. A 375 (2017) 20160088, http://dx.doi.org/10.1098/rsta.2016.0088.
[40] J. Jímenez, G. Kawahara, M.P. Simens, M. Nagata, M. Shiba, Characterization of near-wall turbulence in terms of equilibrium and "burstin" solutions, Phys. Fluids 17 (2005) 015105, http://dx.doi.org/10.1063/1.1825451.
[41] M. Lee, R.D. Moser, Direct numerical simulation of turbulent channel flow up to $Re_\tau \approx 5200$, J. Fluid Mech. 774 (2015) 395–415, http://dx.doi.org/10.1017/jfm.2015.268.
[42] S.B. Pope, Turbulent Flows, Cambridge University Press, 2000, http://dx.doi.org/10.1017/CBO9780511840531.
[43] A.J. Smits, B.J. McKeon, I. Marusic, High-Reynolds number wall turbulence, Annu. Rev. Fluid Mech. 43 (2011) 353–375, http://dx.doi.org/10.1146/annurev-fluid-122109-160753.
[44] I. Marusic, J.P. Monty, M. Hultmark, A.J. Smits, On the logarithmic region in wall turbulence, J. Fluid Mech. 716 (2013) R3, http://dx.doi.org/10.1017/jfm.2012.511.
[45] M.D. Warholic, H. Massah, T.J. Hanratty, Influence of drag-reducing polymers on turbulence: effects of Reynolds number, concentration and mixing, Exp. Fluids 27 (1999) 461–472, http://dx.doi.org/10.1007/s003480050371.
[46] P. Fife, Scaling Approaches to Steady Wall-Induced Turbulence, Technical Report, The University of Utah, 2006, URL: http://www.math.utah.edu/~fife/revarticle.pdf.
[47] M. Själander, M. Jahre, G. Tufte, N. Reissmann, EPIC: An energy-efficient, high-performance GPGPU computing research infrastructure, 2019, arXiv:1912.05848.